Focused surface acoustic waves induced microdroplets generation and its application for microgels

Shaobo Jin[a], Xueyong Wei*[a], Zhen Liu[a], Juan Ren[a], Zhuangde Jiang [a], Chris Abell[b] and Ziyi Yu*[b]

a.State Key Laboratory for Manufacturing Systems Engineering, Xi ́an Jiaotong University, Xi ́an, 710049, China; E-mail: seanwei@mail.xjtu.edu.cn
b.Department of Chemistry, University of Cambridge, Lensfield Road, Cambridge CB2 1EW, UK; E-mail:zy251@cam.ac.uk.

Abstract

We demonstrate a novel microdroplets generation method by using focused surface acoustic waves (FSAW). The method differs from previous work in the mechanism and the geometry structure of the chip, which is depend on FSAW rather than flow shearing. The acoustic radiation force arising from FSAW acts on the oil-water interface, breaking up the water into microdroplets whose size can be controlled by tuning the driving voltage and frequency of FSAW. This approach overcomes the limitation of microchannel structure and capillary number of the traditional microfluidic droplets formation methods, which enables a fully electrical control of microdroplets size, with a good uniformity. Further, the FSAW-induced microdroplets are used as templates to prepare microgels with uniform size, offering a new platform for the design and synthesis of monodispersed functional microspheres.

Keywords: microdroplets generation; FSAW; electrical control; microgels

1. Introduction

The use of microdroplets has become a powerful experimental platform in biology, chemistry, medicine, and material preparation. It has been used inter alia for cell analysis and culture, chemical synthesis, drug screening[1-5]. In these applications, various droplet manipulations such as production [6-8], splitting[9-11], merging[9, 12-14], screening[15-17], capturing and releasing[18-20], and motion control[21, 22] have been realized. Of all these processes, microdroplet formation is the most significant in droplet-based microfluidics.

In the process of microdroplets formation, energy needs to be introduced to the interface of two immiscible phases. This categorizes the formation methods into two groups, namely, passive and active. In droplet microfluidics, generation of microdroplets based on passive methods including flow convergence, T-junction and micro capillary have reached a sufficient level of maturity[1-8], which mainly depends on the design of the microfluidic channel. To maintain a good uniformity of microdroplet size, a stable flow velocity or input pressure must be guaranteed. This flow velocity is usually controlled by a peristaltic pump or a syringe pump. In most microfluidic devices, the pressure source is located away from microfluidic chip with a long connecting tubing, introducing time delay caused by the compressibility of the liquid or the channel material[3, 7]. Therefore, it is hard to precisely control droplet size using the passive methods.

On the other hand, active methods using electrical[23-26], thermal[27], magnetic[28, 29] or piezoelectric[3, 30] effects to produce microdroplets have gained popularity because the droplet size can be precisely tuned by simply adjusting the external excitation source. In addition, surface acoustic waves (SAW) have also attracted wide attention[31, 32], due to its attributes, including high energy confinement waves propagating along the surface of the substrate, efficient fluid-structure coupling, and being clean and non- polluting[31, 33, 34]. Consequently, SAW-based microfluidics have been widely used in microdroplet manipulation including splitting[10, 11], merging[14], sorting[16, 17], capturing and releasing[20] and other applications such as fluid and particle manipulation[31, 34, 35], chemical synthesis, and atomization drug delivery [33, 36-41].

However, there are few reports of SAW-based microdroplet formation, although SAW has been used to assist microdroplets formation in passive method. For example, SAW was used like a pump to press the dispersed phase into the continuous phase in a T-junction microchannel, and then the dispersed phase was cut into droplets[7, 8] by the shearing force of the continuous phase flow. SAW was also used to control the microdroplet size in a flow-focusing microfluidic device through increasing the flow pressure in the lower inlet channel[42, 43]. The microdroplet is formed because of the hydrodynamic shearing force from the continuous phase flow rather than the direct effect of SAW.

In this work, we demonstrate a method of microdroplets generation based on new mechanism of active generation and microfluidic chip design. The microdroplets generation is depend on the direct shear effect of focused surface acoustic waves (FSAW) rather than flow shear of continuous phase. The acoustic radiation force arising from FSAW acts on the oil-water interface, breaking up the continuous water flow into microdroplets whose size can be precisely controlled by a simple tuning of the driving frequency and voltage of FSAW. This technique is easy to implement and has been successfully applied to generate droplets and polyacrylamide hydrogel microgels.

2. Methods and operation principle

2.1 Device design

The FSAW-based microdroplet generation device comprises two parts including focused interdigital transducers (FIDTs) and a bonded PDMS channel on the lithium niobate ($LiNbO_3$) substrate, as shown in Fig.1(a). The width of left channel and right channel are 40 μm and 100 μm, respectively, with the same channel depth of 80 μm. FSAW as an enhancement of SAW excited by FIDTs with arc electrodes has been reported with characteristics of high energy intensity, high beam-width compression and localized area[44]. In this work, the degree of arc of FIDTs is set to be 60 ° and the resultant FSAW is considered to have smaller energy attenuation, higher focused energy and longer propagation distance[45]. In the experiment, a driving electrical signal from a signal generator (33250A, Agilent, USA) was first amplified by a power amplifier (BA4850, NF Corporation, Japan) and then applied on the FIDTs. The $LiNbO_3$ substrate is stretched periodically due to the migration of the charge centre under the action of electric field, resulting FSAW as shown in Fig.1 (b).

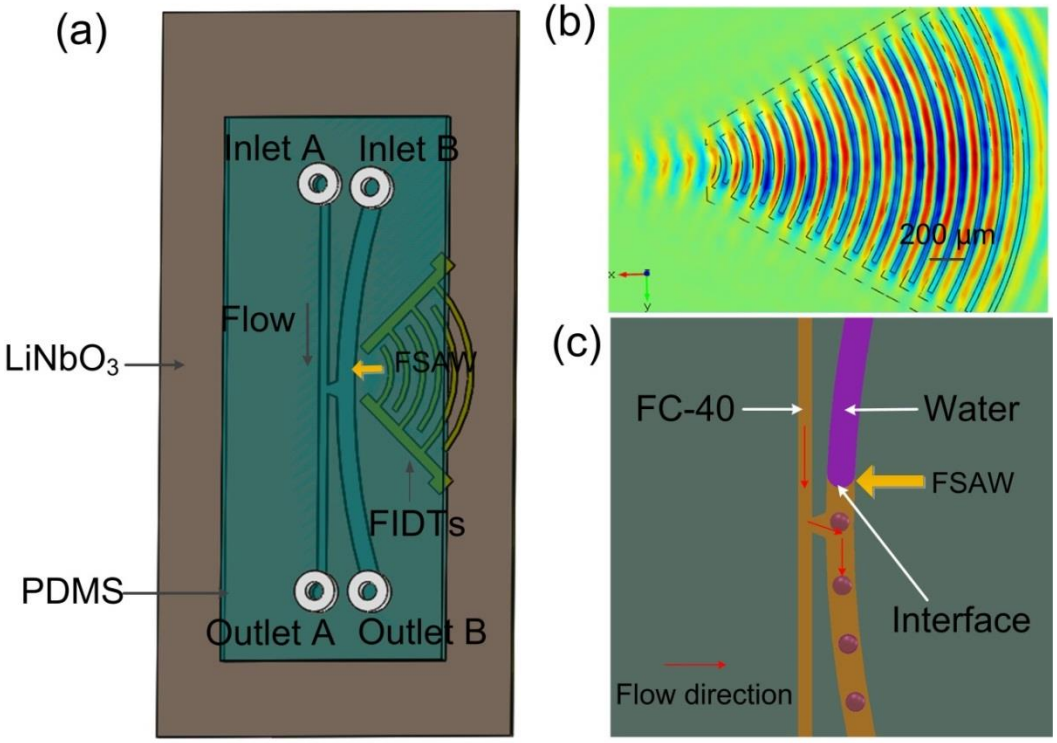

Fig.1 (a) Schematic diagram of a FSAW-based microdroplet generation device comprising a PDMS channel chip and a FIDTs. The PDMS channel comprises two channels, two inlets and two outlets. The FIDTs produce FSAW directed at the two-phase interface. (b) The simulation result of FSAW actuated by FIDTs. (c) The formation of the two-phase interface when FC-40, the deionized water are pumped into inlet A, inlet B and generation of microdroplets using FSAW.

FC-40 oil is pumped into the inlet A as the continuous phase, and the deionized water is pumped into the inlet B as dispersed phase using the flow control system (MFCS™-EZ, Fluigent, France). By adjusting the inlet pressure of inlet A and inlet B, the left channel and part of the right channel are filled FC-40, part of the right channel is filled the deionized water. When the pressure in the channel is balanced, a two-phase interface is formed in the convergence location of FSAW. Then when FSAW is on, the two-phase interface is squeezed, which causes the dispersed phase to move into the continuous phase and the

formation of droplets, as shown in Fig1.(c), the detailed process analysis will be in the chapter 2.3. The experimental process was recorded by an image acquisition system including a microscope (M330-M100, AOSVI, China), a high speed CCD camera (MIROEX4-4096MC, Phantom, USA).

2.2 Fabrication of a FSAW microfluidic chip

The FSAW microfluidic chip shown in Fig.1(a) was fabricated by three steps. In the first step, the FIDTs were made by a lift-off process. First, EPG535 photoresist (Everlight Chemical, Taiwan, China) was patterned on the LiNbO3 substrate using standard lithography, and then the metal layers (Cr/Au,50/300 nm) were deposited by magnetron sputtering (Explorer 14, Denton Vacuum, USA) to form the FIDTs. Finally, the photoresist was removed by acetone (99.8%, XL, China). The FIDTs have 15 pairs of electrodes with uniform width and spacing of 25 μm giving a frequency of 39.96 MHz. In the second step, the PDMS microchannel was fabricated using a soft lithography technology. First, a microchannel mould was fabricated with SU-8 photoresist (Micro Chem, USA). Then the PDMS pre-polymer base (Sylgard 184, Dow Corning, USA) was mixed with the curing agent by a weight ratio of 10:1 and poured into the channel mould. The PDMS channel was peeled off from the mould after curing at 75 ℃ for 2 hours. In the third step, to bond the PDMS channel on the LiNbO3 substrate with FIDTs, an oxygen plasma treatment of 40 s (PDC-32G, Harrick, USA) was carried out and then the surfaces were pressed together with an accurate alignment, followed by a post-baking at 150 ℃ for 3 hours to make a complete bonding.

2.3 Operating principle

The process of microdroplet formation is shown in Fig2. When FSAW is off, a stable interface between FC-40 and water is formed in the focused region of SAW. Its position can be changed through an accurate adjustment of the inlet pressure of inlet A and inlet B. Accordingly, there are no droplets generation because of the stable interface without external perturbations as shown in Fig.2(a).

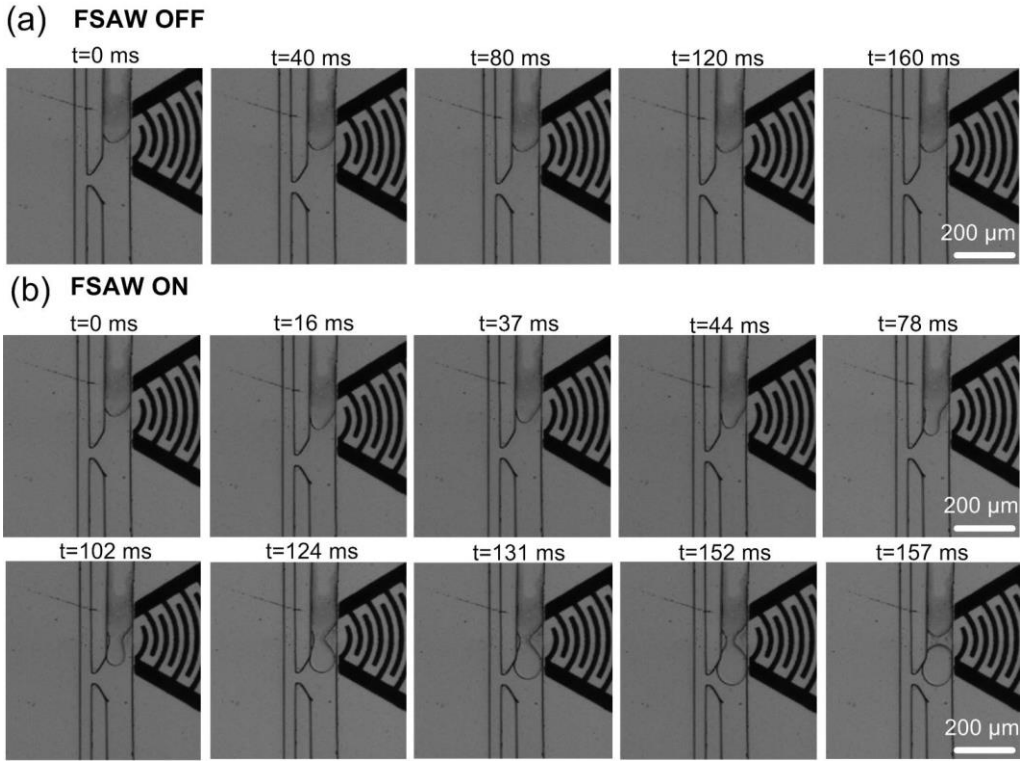

Fig.2 (a) The two-phase flow interface remains stable in the absence of FSAW. (b) Experimental images of FSAW-induced droplet formation within 157 ms. The applied frequency of FSAW is 35.4 MHz, and the input pressure of channel A and inlet B are 68 mbar and 42 mbar respectively.

When FSAW is on, the oil/water interface starts to deform from a convex to a concave shape, forming a neck under the actuation of the acoustic radiation force. The droplet comes to shape at 78 ms and its size continues to grow as the balance of interface is perturbed. At 102 ms, the width of neck region starts to shrink. This lasts about 50 ms until the droplet breaks up from the bulk flow in right channel. A droplet is

thus generated and driven into downstream by the continuous phase flow in left channel. The droplets are completely formed by the FSAW and can be continuously generated (see video1).

According to the results in Fig.2, the process of microdroplet formation is divided into three stages, including the deformation of the two-phase interface in 0-78 ms(Fig.3(a), Fig.3(b)), the growth of the microdroplet in 78-128 ms(Fig.3(c)), and the neck-breaking of the microdroplet in 128-157 ms (Fig.3(d)).

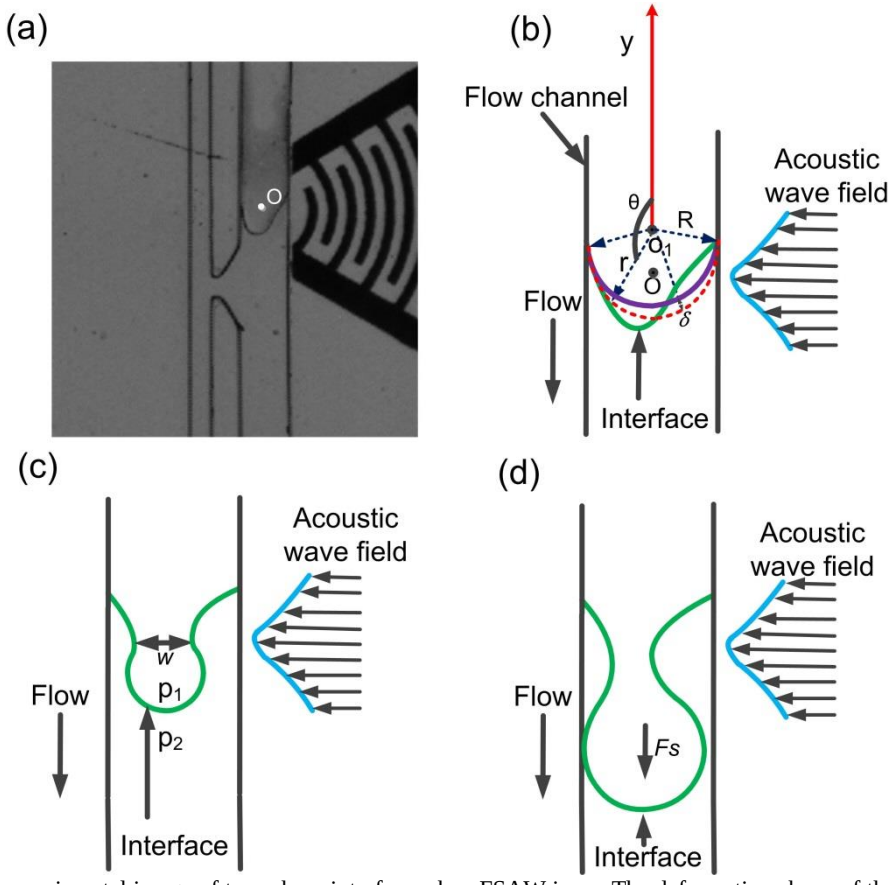

Fig.3 (a) The experimental image of two-phase interface when FSAW is on. The deformation shape of the two-phase interface in the deformation stage of microdroplet. Point O is the acoustic convergence point of FIDTs. (b) The deformation model of the two-phase interface when FSAW is off and on in the first stage, the purple curve line represents the shape before deformation, the green line represents the deformation shape in the deformation stage, the red dotted line is the deformation shape of two-phase interface in uniform acoustic field, point o_1 is the circle center of the fitting interface. (c) The deformation shape of the two-phase interface in the growth stage. (d) The deformation shape of the two-phase interface in the neck-breaking stage. F_s is the acoustic radiant force produced by FSAW.

In the deformation stage, the two-phase flow interface starts to deform when the propagating FSAW acts on it. There is both acoustic radiation force and acoustic streaming force in the process. Singh et al. found that the acoustic streaming drag force induced by FSAW accounts for 10% of the acoustic radiation force[44]. Park et al. pointed out that the acoustic radiation effect was the key mechanism responsible for the acoustic droplet splitting and steering[11]. IssENMANN et al. further proved that the deformation of two-phase interface in surface acoustic wave field was due to the acoustic radiation force, rather than the acoustic streaming effect, successfully verifying the Langevin radiation pressure model[46]. Therefore, the acoustic radiation effect is the main driving force of the microdroplet formation in this work. For a given frequency of FSAW, the amplitudes of acoustic radiation force and acoustic radiation pressure induced by FSAW pointed out the acoustic radiation force are proportional to the square of peak-to-peak value of driving voltage (V_{pp})[11, 47] and its peak-to-peak value:

$$F_a \propto p_a^2 \propto V_{pp}^2 \tag{1}$$

Where F_a is the amplitude of acoustic radiation force, p_a is the amplitude of acoustic radiation pressure p_r.When FSAW acts on the interface of two immiscible fluid, the acoustic radiation pressure acting on the two-phase interface can be given by[7]:

$$p_r = \langle p - p_0 \rangle + \langle I \rangle \tag{2}$$

Where p is the pressure in the fluid (FSAW actuation), p_0 is the pressure in the fluid (without FSAW), I is the energy density in the fluid .The compression of fluid induced by nonlinear propagation of FSAW leads to the increase of the static pressure component $\langle p - p_0 \rangle$ in the fluid. The increase of

static pressure component and nonzero pressure term leads to the deformation of two-phase interface(Fig.3 (a)). We assume the two-phase interface as a spherical surface when SAW is off, the deformation model of the two-phase interface is built as shown in Fig.3 (b). First, we fit the two-phase interface into a circle in the horizontal plane, then set up the polar coordinate system using the circle center of the fitting interface (o_1) as the origin. The droplet surface shape is given in acoustic radiation pressure by Yuren and Marston et al[48], the polar coordinates of each point on the interface after deformation can be expressed as :

$$r(\theta) = R\left[1 - \frac{3R(p_a(\theta))^2}{64\gamma\rho_0 c_0^2}\left(1 + \frac{7}{5}(k_0R)^2\right)(3(\cos\theta)^2 - 1)\right] = R + \delta(\theta) \quad (3)$$

Where r is the polar radius, θ is the polar angle, R is the radius of the fitting circle of the two-phase interface, $p_a(\theta)$ is the amplitude of acoustic radiation pressure on any position of the two-phase interface, γ is the surface tension, ρ_0,c_0 are the density and speed of sound in oil, k_0 is the acoustic wave number in droplet, δ is the deformation value under SAW.

If the acoustic field is uniform, $p_a(\theta)$ can be assumed to be a fixed value. So the Eq.(3) can be changed into:

$$r(\theta) = \left(R - \frac{A}{2}\right)\left[1 - \frac{3A}{2R-A}cos\ 2\theta\right] \quad (4)$$

Where

$$A = \frac{3R^2p_a^2}{64\gamma\rho_0c_0^2}\left(1 + \frac{7}{5}(k_0R)^2\right) \quad \text{is a constant value.}$$

From Eq.(4), the cross section deformation of the two-phase interface can be seen as an ellipsoid, which has the largest deformation at the bottom of the two-phase interface($r_{bottom} = r(-\pi)$).So the uniform acoustic radiation field would result in the deformation of the two-phase interface would as an oblate shape as shown the red dotted line (Fig.3 (b)). But in this paper, we use the FSAW to act on the two-phase interface, the acoustic field is non-uniform. The acoustic amplitude distributes like a gaussian distribution in the y direction, and the acoustic amplitude increases as the applied voltage increases, the location of the strongest acoustic field is the acoustic convergence point (O). So due to the FSAW and squeezing force, the location of largest deformation is in the position of acoustic convergence and the bottom of the two-phase interface. When acoustic radiation pressure and the inner pressure of the fluid reach the balance in the horizontal direction, it forms the neck with the width (w) as shown in Fig.3 (c). It is clear that the stronger the acoustic pressure field, the larger the deformation of the two-phase interface, the smaller the width of the neck.

According to Young-Laplace equation, before FSAW is on, the local pressure difference on both sides of interface and interfacial tension are balanced in the vertical direction. When FSAW travels along the substrate and propagates into the fluid, due to the deflection and reflection of FSAW in the two-phase interface, there is a increased difference Δp_r before and after adding the sound field on both sides fluid of the interface in the vertical direction (Fig.3 (a))[10, 49]:

$$\Delta p_r = p_1 - p_2 - \gamma(1/R + 1/h) \quad (5)$$

Where p_1, p_2 are the local pressure beside the two-phase interface, γ is the interfacial tension, is the mean curvature of the two-phase interface, R is the curvature radius of the two-phase interface when FSAW is off, h is the channel depth. When $\Delta p_r = 0$, the local pressure difference $(p_1 - p_2)$ on both sides of interface and interfacial tension $\left(\gamma(1/R + 1/h)\right)$ are equal, the two-phase interface is stable. When $\Delta p_r \neq 0$, namely FSAW is on, the increased difference will break the pressure balance on both sides fluid of the interface, resulting in the growth volume (V_P) of droplet in the second stage. During the time (τ) of droplet formation, the growth volume (V_p) of droplet is the product of time duration and the average water flow rate ($\overline{Q_w}$) given by[50]:

$$V_p \sim \tau\overline{Q_w} \quad (6)$$

The average water flow rate depends on the width of the neck and difference Δp_r, but there is no exact equation to represent that due to non-uniform distribution of FSAW and the deformation of the interface yet. The deflection and reflection in the two-phase interface in the neck-breaking stage, will exists an acoustic gradient force F_s due to the inhomogeneity of acoustic pressure field[11]. If the shape of microdroplet is simplified as an ideal sphere, then the acoustic gradient force can be expressed as (Fig.3 (c)):

$$F_s = \alpha \int_0^{2\pi}\int_0^{\pi/2} I([Asin2\theta_1 - \beta])R_1{}^2 sin2\theta_1 d\theta_1 d\varphi \quad (7)$$

$$\beta = T^2\frac{sin2(\theta_1-\theta_2)+Asin2\theta_1}{1+A^2+2Acos2\theta_2},$$

Where, θ_1 is the incident angle, θ_2 is reflection angle, φ is the polar angle, R_1 is the radius of the sphere, A and T are the Rayleigh reflection coefficients. The acoustic gradient force will separate the microdroplet from the dispersed phase and push the microdroplet into the continuous phase. But if the

acoustic radiation force is too large, the interface will be completely pressed back to the original side so that the droplets can not be generated. If it is too small, it will not be enough to provide the increased pressure difference of the droplet and meet the requirement of the droplet formation. Obviously, the generation of this method is different from the traditional fluid shear and depends, which entirely depend on the acoustic radiation force and its distribution. The essence of the microdroplets production is due to the deformation of two-phase interface caused by FSAW. The size of microdroplets can be simply tuned by varying the applied frequency and driving voltage of FSAW. Experiments described below were carried out to explore these parametric effects.

3. Results and discussion

3.1 Effect of driving frequency on the size of FSAW-induced microdroplets

To study the influence of FSAW frequency on the size of microdroplets, the peak-to-peak value of the driving voltage (V_{pp}), and the inlet pressures of inlet A (P_A) and inlet B (P_B) were fixed at constant values of 32.5 V, 77 mbar and 40 mbar respectively. The driving frequency of FSAWs was tuned from 34.4 MHz to 36.4 MHz, which was found to be the optimal working range around the FIDTs' resonant frequency of 35.4 MHz. Fig.4 (a) shows the effect of applied driving frequency on the droplet size. As one can see, the droplet is elongated in the channel and its length is about 325 μm at a frequency of 34.5 MHz. When the frequency is increased close to the resonant frequency, the size of droplet continuously decreases. The shape of droplet is close to spherical at 35.4 MHz and the diameter is about 100 μm. If the frequency is increased away from resonance frequency, the size of the droplet increases again. Fig.4 (b) shows the relationship between the droplet size and the driving frequency, in which there is a clear valley in the data at the resonance frequency point. It is well known that, the closer of frequency of driving signal to the resonance frequency, the more efficient of conversion from electrical energy to FSAW energy, which induce a stronger acoustic radiation pressure. According to the Eq.(1-7), a stronger acoustic radiation force will induce a larger deformation of the oil/water interface, leading to a narrower neck region in the droplet formation process. As the above analysis, the effect of driving frequency on the neck width is as shown in Fig.4 (c). In addition, the relationship between the time (τ) of microdroples formation and input frequency is obtained as the driving voltage increases (Fig.4 (d)). The changing trend of the neck width, time of microdroplets formation, and droplet length as input frequency increase is consistent. Clearly, a narrower neck region and shorter time process at the resonance frequency point lead to the generation of smaller droplets. When the applied driving frequency is nearly 35.4 MHz, the microdroplets formation has a shortest formation time and narrowest neck, inducing the smallest microdroplets generation.

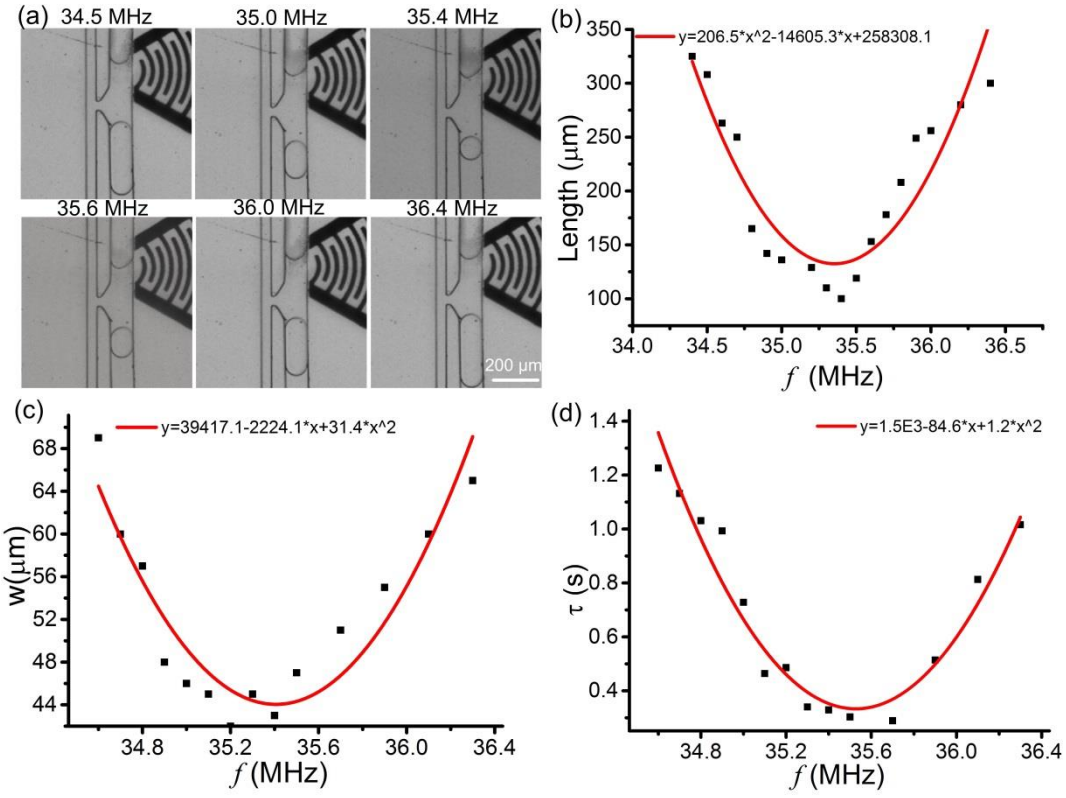

Fig.4 (a) Experimental images of the droplet generation size vary with the applied frequency at the inlet A input pressure of 77 mbar, the inlet B input pressure of 40mbar, the applied voltage of 32.5 V. (b) The droplet length is plotted for varying input frequency in different conditions. (c) The relationship between the neck width of droplet formation and varying input frequency at the inlet A input pressure of 77 mbar, the inlet B input pressure of 40mbar, the applied voltage of 32.5 V. (d) The relationship between the time and varying input frequency.

3.2 Effect of driving voltage on the size of FSAW- induced microdroplets

The experiment was carried out by fixing the driving frequency at 35.4 MHz and the inlet pressure of inlet A and inlet B at 71 mbar and 35 mbar respectively. Fig.5 (a) shows the images of the generated microdroplets at different driving voltages. The length of microdroplet is about 186 μm at V_{pp} of 30 V and it keeps decreasing as the driving voltage increased (see video2). A spherical droplet comes into shape when the driving voltage is larger than 35 V. A linear relationship between the droplet size and the applied driving voltage is shown in Fig.5 (b). According to Eq.1 to Eq.7, it can be seen the deformation value oil/water interface and the acoustic gradient force induced by acoustic radiation pressure increases as the applied voltage increases, which induces a larger deformation and narrower droplet neck as the driving voltage (V_{pp}) increases(Fig.5 (c)). Furthermore, the shorter time of droplet formation is induced as the driving voltage increases(Fig.5 (d)). The changing trend of the neck width, the time of microdroples formation, and droplet length as input frequency increase is similar. Obviously, according to Eq.6, the narrower neck region and shorter time process as the driving voltage increases lead to the generation of smaller droplets.

However, the driving voltage should be set in a certain range. If the driving voltage is too low, the acoustic radiation force is not enough to deform the interface and no droplet is generated. When the acoustic radiation force is too strong, it acts as a kind of resistance to block the fluid. Jin et al. set up an acoustic field to capture droplets based on this principle[20].

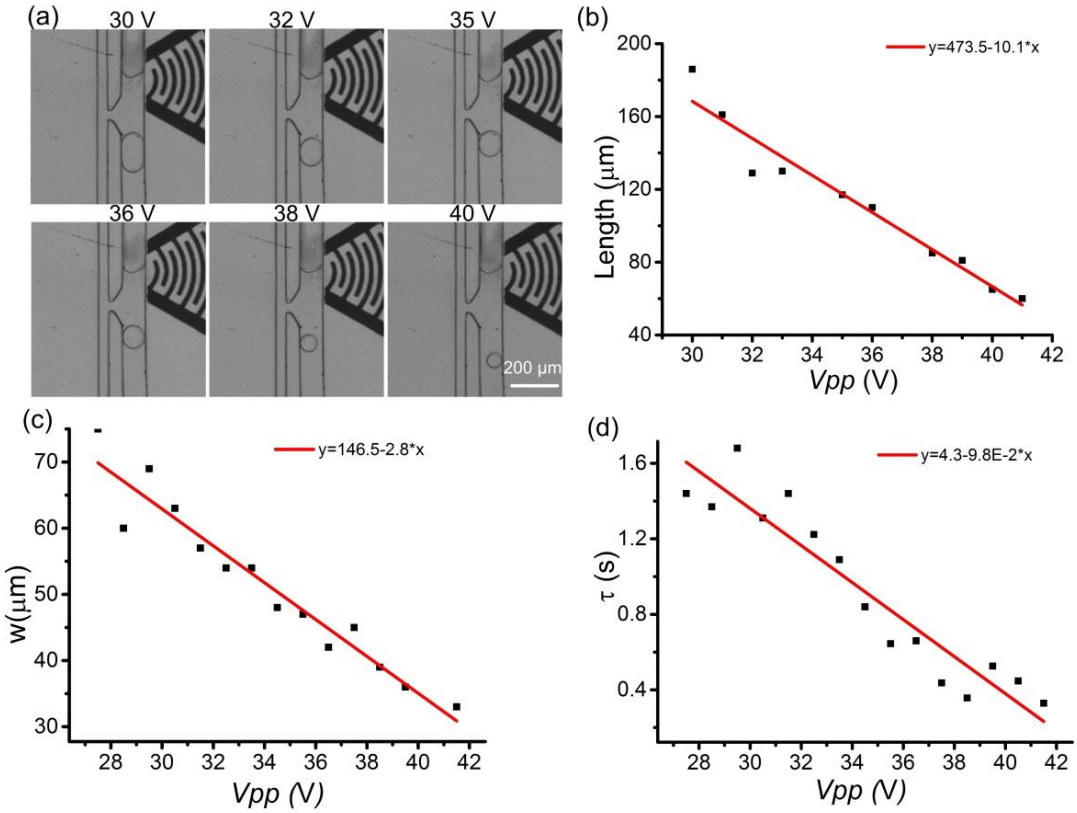

Fig.5 (a) Experimental images of the generated droplet size varying with the applied voltage at a inlet A input pressure of 71 mbar, and inlet B input pressure of 35 mbar, the applied frequency of 35.4MHz. (b) The droplet length is plotted for varying input voltage in different conditions. (c) The relationship between the neck width of droplet formation and varying input frequency at a inlet A input pressure of 71 mbar, and inlet B input pressure of 35 mbar, the applied frequency of 35.4MHz. (d) The relationship between the time and varying input frequency.

3.3 Effect of inlet pressure on the size of FSAW-induced microdroplets

The inlet pressure of inlet A and inlet B can also impact on the size of microdroplets when the driving frequency and voltage are set constant to produce the same FSAW. In the experiment, the inlet pressure of one channel was fixed while the other was adjusted. As shown in Fig.6, the size of droplet decreases as the inlet pressure of inlet A increases, while the size increases as the inlet pressure of inlet B increases. That is because the adjustment of inlet pressure of either inlet A or inlet B will shift the position of the oil/water interface, thus affecting the formation of droplet. Increasing the inlet pressure of inlet A will produce larger flow resistance for the dispersed phase in inlet B and the oil/water interface will withdraw from the FSAW region. According to Eq.3 and Eq.7, this results in a smaller neck and average water flow rate, which induces a smaller amount of bulk flow in inlet B being squeezed into the droplet by the FSAW. On the contrary, increasing the inlet pressure of channel B will push more bulk flow into the FSAW region, leading to larger droplets. However, the inlet pressure of both inlet A and inlet B also must be within a certain range to guarantee the microdroplet formation.

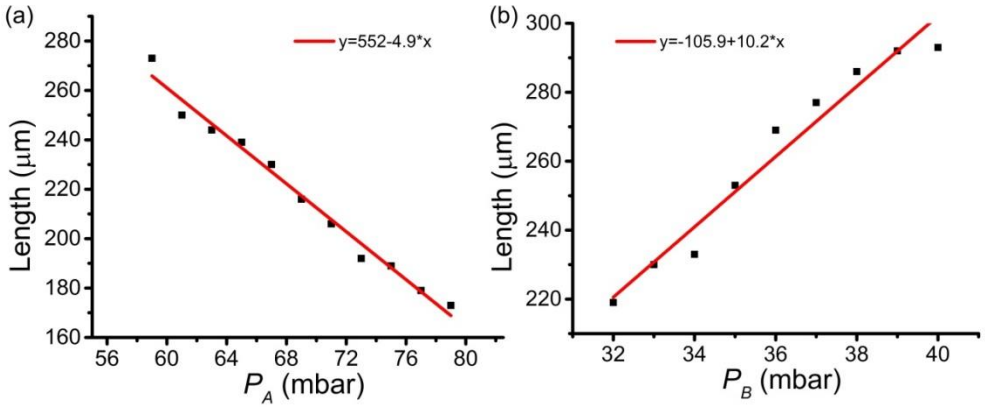

Fig.6 (a) The droplet length is plotted for varying the input pressure of inlet B at the applied voltage of 7.8 V, the applied frequency of 35.4 MHz, the inlet A input pressure of 74 mbar. (b) The droplet length is plotted for various input pressures of inlet A at the applied voltage of 7.8 V, the applied frequency of 35.4 MHz, the inlet A input pressure of 32 mbar.

3.4 Polyacrylamide hydrogel microsphere generation

Hydrogel has emerged as an important class of materials for a wide range of applications in chemistry, medicine and biology[51,52]. Particularly, polyacrylamide hydrogel microsphere (PAMHM) has an excellent porous structure and good biological compatibility, which can be used in biomedical engineering applications such as cell and protein embedding, reagent release control, high-throughput DNA sequencing, and fluorescent tracer agent[53, 54]. The manufacturing methods of PAMHM mainly include reverse suspension polymerization, inverse emulsion polymerization and dispersion polymerization. Each method however has its limitations. For example, inverse emulsion polymerization can only produce nanoscale PAMHM. Reverse suspension polymerization can manufacture micron grade PAMHM, but their uniformity is bad. Practically, a uniform size of PAMHM is important for biomedical applications and therefore a convenient and efficient manufacturing method is needed[54-56].

Passive microdroplet generation methods such as T-junction and micro capillary have been used to synthesize various kinds of microspheres[52, 53, 57, 58]. SAW control is an attractive approach for droplet production and sorting due to its contactless manipulation and good biocompatibility. Biological samples such as cells can be encapsulated in droplets, retaining a high viability even with many hours of exposure to acoustic fields[16].The FIDTs can be located outside of the channel, preventing the electrodes from being in contact with the fluids directly. Furthermore, the FIDTs allows a small footprint suitable for integration into a small microfluidic device[3]. Meanwhile, the FSAW-based microdroplet formation technique in this paper is more flexible in controlling droplet size and production rate, and can be better applied to on-demand droplet generation in some application. The size of the droplets based on FSAW is very uniform and can be generated with a very large range. The production rate and size of droplets can be precisely controlled by a simple tuning of the driving frequency and voltage of FSAW, which will largely promote practical applications of microfluidic droplets and easier realize the integrated automatic control of instrument and equipment. However it is almost impossible for the passive droplet generation to independently control droplet size and generation frequency except by controlling the input pressure of

the input fluid. Compared with the response time of several seconds or even minutes in a passive method, the FSAW-based microdroplet formation technique has a much shorter system response time for stabilized droplet production, which can be down to several milliseconds[4]. Above all, it is believed that the FSAW-based microdroplet formation technique can also be applied to manufacturing microspheres with a broad application prospect.

In this work, the use of FSAW to produce the water-in-oil microdroplets enables the preparation of microgels by polymerization of acrylamide monomers with a crosslinker of bis-acrylamide. As a continuous phase, FC-40 with 0.5% (w/w) surfactant (Pico-SurfTIM2) and 1% (w/w) tetramethylethylenediamine is pumped into the inlet A. The composition of the dispersed phase in inlet B is an aqueous solution containing 50% (w/v) acrylamide, 1% (w/v) bis-acrylamide, and 1% (w/v) ammonium persulfate. As shown in Fig.7 (a) and (b), the FSAW-induced pressure creates a pronounced "neck" of the aqueous solution and it breaks up to form microdroplets in the down-steam continuous phase. The addition of monomers in the aqueous phase does not affect the generation of the microdroplets, which exhibited a narrow size distribution with a coefficient of variation (C.V.) of 4.7% (Fig.7 (c)). The microdroplets were collected either on a glass slide or in an Eppendorf tube for 1 hour incubation. Upon polymerization, the microdroplets are solidified and turned into microgels (Fig.7 (d)). The microgel beads can be washed out from the FC-40 oil and then can be dispersed in aqueous phase.

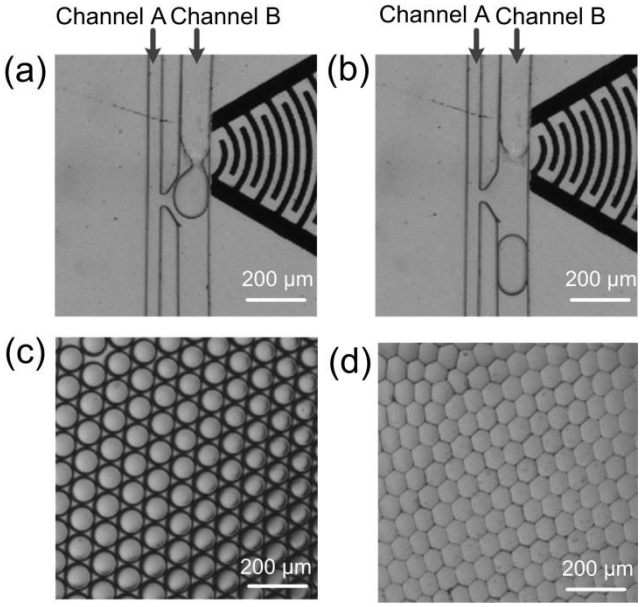

Fig.7 (a-b) Experimental images of liquid microsphere generation induced by FSAW at a inlet A input pressure of 80 mbar, a inlet B input pressure of 50 mbar, and an applied voltage of 7V, the applied frequency is 35.4 MHz. (c-d) The experimental images of microspheres shape vary with time. This last caption needs improving.

4. Conclusions

In summary, we report a new microdroplet formation method based on FSAW-driven microfluidics. The mechanism and the process of the microdroplet formation under FSAW were investigated. The size of the microdroplet generated was primarily determined by the interface deformation and the flow rate of the dispersed phase. This can be controlled by adjusting the frequency and driving voltage of FSAW. The method uses acoustic radiation force to squeeze the continuous water flow into microdroplets, which is simple and easy to implement. It can overcome the limitation of microchannel structure and capillary number. Further, monodispersed polyacrylamide hydrogel microspheres were prepared by FSAW-driven microfluidic droplets. Compared with traditional methods, it shows a better control of size uniformity and it is expected to be a promising method for microgels generation[58].

Acknowledgements

This project is financially supported by the National Natural Science Foundation of China (51575439 and 51711530237), Royal Society-Newton Mobility Grant (IE161541), and 111 project (B12016). We also appreciate the support from the International Joint Laboratory for Micro/Nano Manufacturing and

Measurement Technologies and the State Key Laboratory for Manufacturing Systems Engineering (sklms2017006). We thank Tina Leontidou's comments of this manuscript.

References:

1. J. Wang, Y. Li, X. Wang, J. Wang, H. Tian, P. Zhao, Y. Tian, Y. Gu, L. Wang and C. Wang, Micromachines. 8(2017) 22.
2. S. Mashaghi, A. Abbaspourrad, D. A. Weitz and A. M. V. Oijen, Trac Trends in Analytical Chemistry. 82(2016) 118-125.
3. Z. Z. Chong, S. H. Tan, A. M. GaÃ Ã N-Calvo, S. B. Tor, N. H. Loh and N. T. Nguyen, Lab Chip. 16(2016) 35-58.
4. Z. Zhu and C. J. Yang, Accounts Chem Res. 50(2017) 22-31.
5. N. Wen, Z. Zhao, B. Fan, D. Chen, D. Men, J. Wang and J. Chen, Molecules. 21(2016) 881.
6. S. A. Nabavi, G. T. Vladisavljević, S. Gu and E. E. Ekanem, Chem Eng Sci. 130(2015) 183-196.
7. D. J. Collins, T. Alan, K. Helmerson and A. Neild, Lab Chip.13(2013) 3225-3231.
8. J. C. Brenker, D. J. Collins, P. H. Van, T. Alan and A. Neild, Lab Chip. 16(2016) 1675-1683.
9. H. Geng, J. Feng, L. M. Stabryla and S. K. Cho, Lab Chip. 17(2017) 1060-1068.
10. J. H. Jung, G. Destgeer, B. Ha, J. Park and H. J. Sung, Lab Chip. 16(2016) 3235-3243.
11. J. Park, J. H. Jung, K. Park, G. Destgeer, H. Ahmed, R. Ahmad and H. J. Sung, Lab Chip. 18(2018) 422-432.
12. X. Niu, S. Gulati, J. B. Edel and A. J. Demello, Lab Chip. 8(2008) 1837-1841.
13. S. Lee, H. Kim, D. J. Won, J. Lee and J. Kim, Microfluidics & Nanofluidics. 20(2016) 1.
14. M. Sesen, T. Alan and A. Neild, Lab Chip, 4(2014), 3325-3333.
15. H. V. Phan, T. Alan and A. Neild, Anal Chem, 88(2016), 5696-5703.
16. H. D. Xi, H. Zheng, W. Guo, A. M. Gañáncalvo, Y. Ai, C. W. Tsao, J. Zhou, W. Li, Y. Huang and N. T. Nguyen, Lab Chip. 17(2017), 751-771.
17. S. Li, X. Ding, F. Guo, Y. Chen, M. I. Lapsley, S. C. S. Lin, L. Wang, J. P. Mccoy, C. E. Cameron and T. J. Huang, Anal Chem. 85(2013), 5468-5474.
18. W. Xu, A. Palumbo, J. Xu, Y. Jiang, C. H. Choi and E. H. Yang, Acs Applied Materials & Interfaces. 9(2017) 23119-23127.
19. M. Courtney, X. Chen, S. Chan, T. Mohamed, P. P. N. Rao and C. L. Ren, Anal Chem. 89(2017), 910-915.
20. H. J. Jin, G. Destgeer, J. Park, H. Ahmed, K. Park and H. J. Sung, Anal Chem. 89(2017) 2211-2215.
21. X. Man and M. Doi, Phys.rev.lett. 119(2017) 044502.
22. P. Sartori, D. Quagliati, S. Varagnolo, M. Pierno, G. Mistura, F. Magaletti and C. M. Casciola, New J Phys. 17(2015) 113017.
23. H. Gu, M. H. G. Duits and F. Mugele, Lab Chip. 10(2010) 1550-1556.
24. E. Castro-Hernández, P. Garcá-Sánchez, S. H. Tan, A. M. Gañán-Calvo, J. C. Baret and A. Ramos, Microfluidics & Nanofluidics. 19(2015) 787-794.
25. D. R. Link, E. Graslandmongrain, A. Duri, F. Sarrazin, Z. Cheng, G. Cristobal, M. Marquez and D. A. Weitz, Angewandte Chemie. 45(2006) 2556-2560.
26. I. M. Chen, H. H. Tsai, C. W. Chang, G. Zheng and Y. C. Su, Sensors & Actuators B Chemical. 260(2018) 541-553.
27. N. T. Nguyen, T. H. Ting, Y. F. Yap, T. N. Wong, C. K. Chai, W. L. Ong, J. Zhou, S. H. Tan and L. Yobas, Appl Phys Lett. 91(2007) 084102.
28. Y. Wu, T. Fu, Y. Ma and H. Z. Li, Soft Matter. 9(2013) 9792-9798.
29. J. Liu, Y. F. Yap and N. T. Nguyen, Phys.Fluids. 23(2011) 072008.
30. Y. N. Cheung and H. Qiu, Appl Phys Lett. 97(2010) 133111.
31. L. Y. Yeo and J. R. Friend, Annu Rev Fluid Mech. 46(2014) 379-406.
32. G. Maltezos, M. Johnston, K. Taganov, C. Srichantaratsamee, J. Gorman, D. Baltimore, W. Chantratita and A. Scherer, Appl Phys Lett. 97(2010) 264101.
33. A. Barani, H. Paktinat, M. Janmaleki, A. Mohammadi, P. Mosaddegh, A. Fadaei-Tehrani and A. Sanati-Nezhad, Biosens Bioelectron. 85(2016) 714-725.
34. X. Ding, P. Li, S. C. Lin, Z. S. Stratton, N. Nama, F. Guo, D. Slotcavage, X. Mao, J. Shi and F. Costanzo, Lab Chip. 13(2013) 3626-3649.
35. S. C. Lin, X. Mao and T. J. Huang, Lab Chip. 12(2012) 2766-2770.
36. S. S. Guo, L. B. Zhao, K. Zhang and K. H. Lam, Appl. Phys. Lett. 92(2008) 213901.
37. Z. Luo, H. Chen, T. Wang, D. Zhou, M. Lu, M. He, M. Fang and K. Cen, Powder Technology. 312(2017) 21-28.
38. J. Nam, H. Lim and S. Shin, Korea-Australia Rheology Journal. 23(2011) 255-267.
39. N. Sivanantha, C. Ma, D. J. Collins, M. Sesen, J. Brenker, R. L. Coppel, A. Neild and T. Alan, Physics Procedia. 70(2015) 18-20.
40. A. Qi, J. R. Friend, L. Y. Yeo, D. A. Morton, M. P. Mcintosh and L. Spiccia, Lab Chip. 9(2009) 2184-2193.
41. K. Kulkarni, J. Friend, L. Yeo and P. Perlmutter, Lab Chip. 9(2009) 754-755.
42. L. Schmid and T. Franke, Lab Chip. 13(2013) 1691-1694.
43. L. Schmid and T. Franke, Appl Phys Lett. 104(2014) 133501.
44. R. Singh, S. K. Sankaranarayanan and V. R. Bhethanabotla, J Appl Phys. 107(2010) 024503.
45. S. K. Sankaranarayanan and V. R. Bhethanabotla, J Appl Phys. 103(2008) 064518.
46. B. Issenmann, A. Nicolas, R. Wunenburger, S. Manneville and J. P. Delville, Epl. 83(2008) 34002.

47. H. Bruus, Lab Chip. 12(2012) 1014-1021.
48. Y. Tian, R. G. Holt and R. E. Apfel, J Acoust Soc Am. 93(1993) 3096-3104.
49. A. D. Rey, J Chem Phys. 113(2000) 10820-10822.
50. T. Glawdel and C. L. Ren, Physical Review E. 85(2012) 016322.
51. S. Jung, J. H. Abel, J. L. Starger and H. Yi, Biomacromolecules. 17(2016) 2427-2436.
52. J. Zhang, Y. Cheng, H. Yuan, Z. Yan, Y. Liu, F. Jing and D. Wu, New Chemical Materials. 45(2017) 107-109.
53. X. Zhao, S. Liu, L. Yildirimer, H. Zhao, R. Ding, H. Wang, W. Cui and D. Weitz, Adv. Funct. Mater. 26(2016) 2809-2819.
54. N. A. Peppas, J. Z. Hilt, A. Khademhosseini and R. Langer, Adv Mater. 18(2006) 1345-1360.
55. N. Wang, Y. Li, Y. Zhang, Y. Liao and W. Liu, Langmuir. 30(2014) 11823-11823.
56. X. Qian, N. Wang, Y. Li, J. Zhang, Z. Xu and Y. Long, Langmuir. 30(2014) 10766-10771.
57. T. Watanabe, T. Ono and Y. Kimura, Soft Matter. 7(2011) 9894-9897.
58. R. Samimi, M. Salarian, W. Z. Xu, E. M. K. Lui and P. A. Charpentier, Ind Eng Chem Res. 53(2014) 11333-11344.